

J/ψ suppression at forward rapidity in Au+Au collisions at $\sqrt{s_{NN}}=39$ and 62.4 GeV

A. Adare,¹¹ C. Aidala,³⁴ N.N. Ajitanand,⁵⁴ Y. Akiba,^{48,49} R. Akimoto,¹⁰ H. Al-Ta'ani,⁴³ J. Alexander,⁵⁴ A. Angerami,¹² K. Aoki,⁴⁸ N. Apadula,⁵⁵ Y. Aramaki,^{10,48} H. Asano,^{31,48} E.C. Aschenauer,⁶ E.T. Atomssa,⁵⁵ T.C. Awes,⁴⁵ B. Azmoun,⁶ V. Babintsev,²² M. Bai,⁵ B. Bannier,⁵⁵ K.N. Barish,⁷ B. Bassalleck,⁴² S. Bathe,^{4,49} V. Baublis,⁴⁷ S. Baumgart,⁴⁸ A. Bazilevsky,⁶ R. Belmont,⁵⁹ A. Berdnikov,⁵¹ Y. Berdnikov,⁵¹ X. Bing,⁴⁴ D.S. Blau,³⁰ K. Boyle,⁴⁹ M.L. Brooks,³⁴ H. Buesching,⁶ V. Bumazhnov,²² S. Butsyk,⁴² S. Campbell,⁵⁵ P. Castera,⁵⁵ C.-H. Chen,⁵⁵ C.Y. Chi,¹² M. Chiu,⁶ I.J. Choi,²³ J.B. Choi,⁹ S. Choi,⁵³ R.K. Choudhury,³ P. Christiansen,³⁶ T. Chujo,⁵⁸ O. Chvala,⁷ V. Cianciolo,⁴⁵ Z. Citron,⁵⁵ B.A. Cole,¹² M. Connors,⁵⁵ M. Csanád,¹⁶ T. Csörgő,⁶¹ S. Dairaku,^{31,48} A. Datta,³⁸ M.S. Daugherty,¹ G. David,⁶ A. Denisov,²² A. Deshpande,^{49,55} E.J. Desmond,⁶ K.V. Dharmawardane,⁴³ O. Dietzsch,⁵² L. Ding,²⁶ A. Dion,²⁶ M. Donadelli,⁵² O. Drapier,³² A. Drees,⁵⁵ K.A. Drees,⁵ J.M. Durham,⁵⁵ A. Durum,²² L. D'Orazio,³⁷ S. Edwards,⁵ Y.V. Efremenko,⁴⁵ T. Engelmores,¹² A. Enokizono,⁴⁵ S. Esumi,⁵⁸ K.O. Eyser,⁷ B. Fadern,³⁹ D.E. Fields,⁴² M. Finger,⁸ M. Finger, Jr.,⁸ F. Fleuret,³² S.L. Fokin,³⁰ J.E. Frantz,⁴⁴ A. Franz,⁶ A.D. Frawley,¹⁸ Y. Fukao,⁴⁸ T. Fusayasu,⁴¹ K. Gainey,¹ C. Gal,⁵⁵ A. Garishvili,⁵⁶ I. Garishvili,³³ A. Glenn,³³ X. Gong,⁵⁴ M. Gonin,³² Y. Goto,^{48,49} R. Granier de Cassagnac,³² N. Grau,¹² S.V. Greene,⁵⁹ M. Grosse Perdekamp,²³ T. Gunji,¹⁰ L. Guo,³⁴ H.-Å. Gustafsson,^{36,*} T. Hachiya,⁴⁸ J.S. Haggerty,⁶ K.I. Hahn,¹⁷ H. Hamagaki,¹⁰ J. Hanks,¹² K. Hashimoto,^{48,50} E. Haslum,³⁶ R. Hayano,¹⁰ X. He,¹⁹ T.K. Hemmick,⁵⁵ T. Hester,⁷ J.C. Hill,²⁶ R.S. Hollis,⁷ K. Homma,²¹ B. Hong,²⁹ T. Horaguchi,⁵⁸ Y. Hori,¹⁰ S. Huang,⁵⁹ T. Ichihara,^{48,49} H. Iinuma,²⁸ Y. Ikeda,^{48,58} J. Imrek,¹⁵ M. Inaba,⁵⁸ A. Iordanova,⁷ D. Isenhowe,¹ M. Issah,⁵⁹ D. Ivanishev,⁴⁷ B.V. Jacak,^{55,†} M. Javani,¹⁹ J. Jia,^{6,54} X. Jiang,³⁴ B.M. Johnson,⁶ K.S. Joo,⁴⁰ D. Jouan,⁴⁶ J. Kamin,⁵⁵ S. Kaneti,⁵⁵ B.H. Kang,²⁰ J.H. Kang,⁶² J.S. Kang,²⁰ J. Kapustinsky,³⁴ K. Karatsu,^{31,48} M. Kasai,^{48,50} D. Kaway,^{38,49} A.V. Kazantsev,³⁰ T. Kempel,²⁶ A. Khanzadeev,⁴⁷ K.M. Kijima,²¹ B.I. Kim,²⁹ C. Kim,²⁹ D.J. Kim,²⁷ E.-J. Kim,⁹ H.J. Kim,⁶² K.-B. Kim,⁹ Y.-J. Kim,²³ Y.K. Kim,²⁰ E. Kinney,¹¹ Á. Kiss,¹⁶ E. Kistenev,⁶ J. Klatsky,¹⁸ D. Kleinjan,⁷ P. Kline,⁵⁵ Y. Komatsu,¹⁰ B. Komkov,⁴⁷ J. Koster,²³ D. Kotchetkov,⁴⁴ D. Kotov,⁵¹ A. Král,¹³ F. Krizek,²⁷ G.J. Kunde,³⁴ K. Kurita,^{48,50} M. Kurosawa,⁴⁸ Y. Kwon,⁶² G.S. Kyle,⁴³ R. Lacey,⁵⁴ Y.S. Lai,¹² J.G. Lajoie,²⁶ A. Lebedev,²⁶ B. Lee,²⁰ D.M. Lee,³⁴ J. Lee,¹⁷ K.B. Lee,²⁹ K.S. Lee,²⁹ S.H. Lee,⁵⁵ S.R. Lee,⁹ M.J. Leitch,³⁴ M.A.L. Leite,⁵² M. Leitgab,²³ B. Lewis,⁵⁵ S.H. Lim,⁶² L.A. Linden Levy,¹¹ M.X. Liu,³⁴ B. Love,⁵⁹ C.F. Maguire,⁵⁹ Y.I. Makdisi,⁵ M. Makek,⁶⁰ A. Manion,⁵⁵ V.I. Manko,³⁰ E. Mannel,¹² S. Masumoto,¹⁰ M. McCumber,¹¹ P.L. McGaughey,³⁴ D. McGlinchey,¹⁸ C. McKinney,²³ M. Mendoza,⁷ B. Meredith,²³ Y. Miake,⁵⁸ T. Mibe,²⁸ A.C. Mignerey,³⁷ A. Milov,⁶⁰ D.K. Mishra,³ J.T. Mitchell,⁶ Y. Miyachi,^{48,57} S. Miyasaka,^{48,57} A.K. Mohanty,³ H.J. Moon,⁴⁰ D.P. Morrison,⁶ S. Motschwiller,³⁹ T.V. Moukhanova,³⁰ T. Murakami,^{31,48} J. Murata,^{48,50} T. Nagae,³¹ S. Nagamiya,²⁸ J.L. Nagle,¹¹ M.I. Nagy,⁶¹ I. Nakagawa,^{48,49} Y. Nakamiya,²¹ K.R. Nakamura,^{31,48} T. Nakamura,⁴⁸ K. Nakano,^{48,57} C. Nattrass,⁵⁶ A. Nederlof,³⁹ M. Nihashi,^{21,48} R. Nouicer,^{6,49} N. Novitzky,²⁷ A.S. Nyanin,³⁰ E. O'Brien,⁶ C.A. Ogilvie,²⁶ K. Okada,⁴⁹ A. Oskarsson,³⁶ M. Ouchida,^{21,48} K. Ozawa,¹⁰ R. Pak,⁶ V. Pantuev,²⁴ V. Papavassiliou,⁴³ B.H. Park,²⁰ I.H. Park,¹⁷ S.K. Park,²⁹ S.F. Pate,⁴³ L. Patel,¹⁹ H. Pei,²⁶ J.-C. Peng,²³ H. Pereira,¹⁴ D.Yu. Peressounko,³⁰ R. Petti,⁵⁵ C. Pinkenburg,⁶ R.P. Pisani,⁶ M. Proissl,⁵⁵ M.L. Purschke,⁶ H. Qu,¹ J. Rak,²⁷ I. Ravinovich,⁶⁰ K.F. Read,^{45,56} R. Reynolds,⁵⁴ V. Riabov,⁴⁷ Y. Riabov,⁴⁷ E. Richardson,³⁷ D. Roach,⁵⁹ G. Roche,³⁵ S.D. Rolnick,⁷ M. Rosati,²⁶ B. Sahlmueller,⁵⁵ N. Saito,²⁸ T. Sakaguchi,⁶ V. Samsonov,⁴⁷ M. Sano,⁵⁸ M. Sarsour,¹⁹ S. Sawada,²⁸ K. Sedgwick,⁷ R. Seidl,^{48,49} A. Sen,¹⁹ R. Seto,⁷ D. Sharma,⁶⁰ I. Shein,²² T.-A. Shibata,^{48,57} K. Shigaki,²¹ M. Shimomura,⁵⁸ K. Shoji,^{31,48} P. Shukla,³ A. Sickles,⁶ C.L. Silva,²⁶ D. Silvermyr,⁴⁵ K.S. Sim,²⁹ B.K. Singh,² C.P. Singh,² V. Singh,² M. Slunečka,⁸ R.A. Soltz,³³ W.E. Sondheim,³⁴ S.P. Sorensen,⁵⁶ M. Soumya,⁵⁴ I.V. Sourikova,⁶ P.W. Stankus,⁴⁵ E. Stenlund,³⁶ M. Stepanov,³⁸ A. Ster,⁶¹ S.P. Stoll,⁶ T. Sugitate,²¹ A. Sukhanov,⁶ J. Sun,⁵⁵ J. Sziklai,⁶¹ E.M. Takagui,⁵² A. Takahara,¹⁰ A. Taketani,^{48,49} Y. Tanaka,⁴¹ S. Taneja,⁵⁵ K. Tanida,^{49,53} M.J. Tannenbaum,⁶ S. Tarafdar,² A. Taranenko,⁵⁴ E. Tennant,⁴³ H. Themann,⁵⁵ T. Todoroki,^{48,58} L. Tomášek,²⁵ M. Tomášek,^{13,25} H. Torii,²¹ R.S. Towell,¹ I. Tserruya,⁶⁰ Y. Tsuchimoto,¹⁰ T. Tsuji,¹⁰ C. Vale,⁶ H.W. van Hecke,³⁴ M. Vargyas,¹⁶ E. Vazquez-Zambrano,¹² A. Veicht,¹² J. Velkovska,⁵⁹ R. Vértesi,⁶¹ M. Virius,¹³ A. Vossen,²³ V. Vrba,^{13,25} E. Vznuzdaev,⁴⁷ X.R. Wang,⁴³ D. Watanabe,²¹ K. Watanabe,⁵⁸ Y. Watanabe,^{48,49} Y.S. Watanabe,¹⁰ F. Wei,²⁶ R. Wei,⁵⁴ S.N. White,⁶ D. Winter,¹² S. Wolin,²³ C.L. Woody,⁶ M. Wysocki,¹¹ Y.L. Yamaguchi,¹⁰ R. Yang,²³ A. Yanovich,²² J. Ying,¹⁹ S. Yokkaichi,^{48,49} Z. You,³⁴ I. Younus,⁴² I.E. Yushmanov,³⁰ W.A. Zajc,¹² and A. Zelenski⁵

(PHENIX Collaboration)

¹Abilene Christian University, Abilene, Texas 79699, USA²Department of Physics, Banaras Hindu University, Varanasi 221005, India³Bhabha Atomic Research Centre, Bombay 400 085, India

- ⁴Baruch College, City University of New York, New York, New York, 10010 USA
- ⁵Collider-Accelerator Department, Brookhaven National Laboratory, Upton, New York 11973-5000, USA
- ⁶Physics Department, Brookhaven National Laboratory, Upton, New York 11973-5000, USA
- ⁷University of California - Riverside, Riverside, California 92521, USA
- ⁸Charles University, Ovocný trh 5, Praha 1, 116 36, Prague, Czech Republic
- ⁹Chonbuk National University, Jeonju, 561-756, Korea
- ¹⁰Center for Nuclear Study, Graduate School of Science, University of Tokyo, 7-3-1 Hongo, Bunkyo, Tokyo 113-0033, Japan
- ¹¹University of Colorado, Boulder, Colorado 80309, USA
- ¹²Columbia University, New York, New York 10027 and Nevis Laboratories, Irvington, New York 10533, USA
- ¹³Czech Technical University, Zikova 4, 166 36 Prague 6, Czech Republic
- ¹⁴Dapnia, CEA Saclay, F-91191, Gif-sur-Yvette, France
- ¹⁵Debrecen University, H-4010 Debrecen, Egyetem tér 1, Hungary
- ¹⁶ELTE, Eötvös Loránd University, H - 1117 Budapest, Pázmány P. s. 1/A, Hungary
- ¹⁷Ewha Womans University, Seoul 120-750, Korea
- ¹⁸Florida State University, Tallahassee, Florida 32306, USA
- ¹⁹Georgia State University, Atlanta, Georgia 30303, USA
- ²⁰Hanyang University, Seoul 133-792, Korea
- ²¹Hiroshima University, Kagamiyama, Higashi-Hiroshima 739-8526, Japan
- ²²IHEP Protvino, State Research Center of Russian Federation, Institute for High Energy Physics, Protvino, 142281, Russia
- ²³University of Illinois at Urbana-Champaign, Urbana, Illinois 61801, USA
- ²⁴Institute for Nuclear Research of the Russian Academy of Sciences, prospekt 60-letiya Oktyabrya 7a, Moscow 117312, Russia
- ²⁵Institute of Physics, Academy of Sciences of the Czech Republic, Na Slovance 2, 182 21 Prague 8, Czech Republic
- ²⁶Iowa State University, Ames, Iowa 50011, USA
- ²⁷Helsinki Institute of Physics and University of Jyväskylä, P.O.Box 35, FI-40014 Jyväskylä, Finland
- ²⁸KEK, High Energy Accelerator Research Organization, Tsukuba, Ibaraki 305-0801, Japan
- ²⁹Korea University, Seoul, 136-701, Korea
- ³⁰Russian Research Center "Kurchatov Institute", Moscow, 123098 Russia
- ³¹Kyoto University, Kyoto 606-8502, Japan
- ³²Laboratoire Leprince-Ringuet, Ecole Polytechnique, CNRS-IN2P3, Route de Saclay, F-91128, Palaiseau, France
- ³³Lawrence Livermore National Laboratory, Livermore, California 94550, USA
- ³⁴Los Alamos National Laboratory, Los Alamos, New Mexico 87545, USA
- ³⁵LPC, Université Blaise Pascal, CNRS-IN2P3, Clermont-Fd, 63177 Aubiere Cedex, France
- ³⁶Department of Physics, Lund University, Box 118, SE-221 00 Lund, Sweden
- ³⁷University of Maryland, College Park, Maryland 20742, USA
- ³⁸Department of Physics, University of Massachusetts, Amherst, Massachusetts 01003-9337, USA
- ³⁹Muhlenberg College, Allentown, Pennsylvania 18104-5586, USA
- ⁴⁰Myongji University, Yongin, Kyonggido 449-728, Korea
- ⁴¹Nagasaki Institute of Applied Science, Nagasaki-shi, Nagasaki 851-0193, Japan
- ⁴²University of New Mexico, Albuquerque, New Mexico 87131, USA
- ⁴³New Mexico State University, Las Cruces, New Mexico 88003, USA
- ⁴⁴Department of Physics and Astronomy, Ohio University, Athens, Ohio 45701, USA
- ⁴⁵Oak Ridge National Laboratory, Oak Ridge, Tennessee 37831, USA
- ⁴⁶IPN-Orsay, Université Paris Sud, CNRS-IN2P3, BP1, F-91406, Orsay, France
- ⁴⁷PNPI, Petersburg Nuclear Physics Institute, Gatchina, Leningrad region, 188300, Russia
- ⁴⁸RIKEN Nishina Center for Accelerator-Based Science, Wako, Saitama 351-0198, Japan
- ⁴⁹RIKEN BNL Research Center, Brookhaven National Laboratory, Upton, New York 11973-5000, USA
- ⁵⁰Physics Department, Rikkyo University, 3-34-1 Nishi-Ikebukuro, Toshima, Tokyo 171-8501, Japan
- ⁵¹Saint Petersburg State Polytechnic University, St. Petersburg, 195251 Russia
- ⁵²Universidade de São Paulo, Instituto de Física, Caixa Postal 66318, São Paulo CEP05315-970, Brazil
- ⁵³Department of Physics and Astronomy, Seoul National University, Seoul, Korea
- ⁵⁴Chemistry Department, Stony Brook University, SUNY, Stony Brook, New York 11794-3400, USA
- ⁵⁵Department of Physics and Astronomy, Stony Brook University, SUNY, Stony Brook, New York 11794-3400, USA
- ⁵⁶University of Tennessee, Knoxville, Tennessee 37996, USA
- ⁵⁷Department of Physics, Tokyo Institute of Technology, Oh-okayama, Meguro, Tokyo 152-8551, Japan
- ⁵⁸Institute of Physics, University of Tsukuba, Tsukuba, Ibaraki 305, Japan
- ⁵⁹Vanderbilt University, Nashville, Tennessee 37235, USA
- ⁶⁰Weizmann Institute, Rehovot 76100, Israel
- ⁶¹Institute for Particle and Nuclear Physics, Wigner Research Centre for Physics, Hungarian Academy of Sciences (Wigner RCP, RMKI) H-1525 Budapest 114, POBox 49, Budapest, Hungary
- ⁶²Yonsei University, IPAP, Seoul 120-749, Korea

(Dated: August 13, 2012)

We present measurements of the J/ψ invariant yields in $\sqrt{s_{NN}}=39$ and 62.4 GeV Au+Au collisions at forward rapidity ($1.2 < |y| < 2.2$). Invariant yields are presented as a function of both collision

centrality and transverse momentum. Nuclear modifications are obtained for central relative to peripheral Au+Au collisions (R_{CP}) and for various centrality selections in Au+Au relative to scaled $p+p$ cross sections obtained from other measurements (R_{AA}). The observed suppression patterns at 39 and 62.4 GeV are quite similar to those previously measured at 200 GeV. This similar suppression presents a challenge to theoretical models that contain various competing mechanisms with different energy dependencies, some of which cause suppression and others enhancement.

Heavy quarkonia are bound states of charm-anticharm or bottom-antibottom quarks. It was proposed over 25 years ago that these states would be color screened in a quark-gluon plasma (QGP), thus suppressing their final yields in relativistic heavy ion collisions [1]. The NA50 experiment at the CERN-SPS measured a significant suppression of J/ψ and ψ' in Pb+Pb collisions at $\sqrt{s_{NN}} = 17.2$ GeV, which was interpreted as indicating the onset of quark-gluon plasma formation [2]. However, measurements by the PHENIX experiment at the Relativistic Heavy Ion Collider (RHIC) indicated a similar level of nuclear suppression at midrapidity in Au+Au collisions at $\sqrt{s_{NN}} = 200$ GeV [3]. Additional PHENIX results also indicated a larger suppression at forward rapidity $1.2 < |y| < 2.2$ compared with midrapidity, despite the expectation of a higher energy density and temperature for the medium at midrapidity. Perhaps more surprising is the comparison of the recent higher statistics PHENIX forward rapidity J/ψ suppression [4] and the ALICE experiment measurement in Pb+Pb at 2.76 TeV [5] at the Large Hadron Collider (LHC). These results indicate significantly less suppression for the most central Pb+Pb events at the LHC compared with Au+Au events at RHIC. Results at RHIC and the LHC at larger transverse momentum ($p_T > 4$ GeV/ c) [6–8] suggest the opposite, with more suppression at the LHC compared to RHIC.

These measurements contradict an interpretation based solely on color screening, and require the influence of other physics. There is an additional class of effects referred to as “cold nuclear matter” (CNM) effects that are not due to the creation of a hot medium and thus can be probed via $p(d)+A$ collisions. These CNM effects include the modification of the initial incoming flux of quarks and gluons in the nucleus as described by nuclear-modified parton distribution functions (nPDFs) [9], breakup of the J/ψ precursor $c\bar{c}$ state while traversing the nucleus, and initial-state parton energy loss. CNM effects have been studied in detail in $p+A$ collisions at $\sqrt{s_{NN}} = 17$ –42 GeV [10–16], in $d+Au$ collisions at $\sqrt{s_{NN}} = 200$ GeV by the PHENIX experiment [17–19], and $p+A$ results from the LHC are anxiously awaited. In addition, there may be effects in the QGP other than color screening. These include the possible coalescence of originally uncorrelated c and \bar{c} quarks or the recombination of breakup c and \bar{c} pairs resulting in a competing enhancement effect (see for example Refs. [20, 21]). This coalescence effect is ex-

pected to grow as the density of c and \bar{c} increases. A recent review of many of these phenomena is given in Ref. [22].

All of this highlights the importance of measuring J/ψ and other excited quarkonia states over a broad range in $\sqrt{s_{NN}}$; thus varying not only the temperature of the medium, but also the c and \bar{c} production and the cold nuclear matter effects. In this paper, the PHENIX collaboration presents first measurements of invariant yields and suppression for J/ψ at forward rapidity $1.2 < |y| < 2.2$ in Au+Au collisions at $\sqrt{s_{NN}} = 39$ and 62.4 GeV.

I. DATA ANALYSIS

The PHENIX experiment collected data in 2010 for Au+Au collisions at $\sqrt{s_{NN}} = 39$ and 62.4 GeV as part of the RHIC Beam Energy Scan program. After good run selection cuts, the data set includes 2.0×10^8 events at 39 GeV and 5.5×10^8 events at 62.4 GeV. The PHENIX experiment is described in detail in Ref. [23]. The J/ψ measurement at forward rapidity is made via the dimuon decay channel with two forward angle muon spectrometers, as detailed in Ref. [24]. The muon spectrometers have acceptance over the range $1.2 < |\eta| < 2.2$ and over the full azimuth. The two spectrometers comprise an initial hadronic absorber followed by three sets of cathode strip chambers which are inside a magnetic field, referred to as the Muon Tracker (MuTr), and then five planes of Iarocci tubes interleaved with steel absorber plates, referred to as the Muon Identifier (MuID). Muon candidates are found by reconstructing tracks through the magnetic field in the MuTr and matching them to MuID tracks that penetrate through to the last MuID plane.

In Au+Au collisions at $\sqrt{s_{NN}} = 39$ and 62.4 GeV, the events are selected with a minimum bias (MB) trigger utilizing the Beam-Beam Counter (BBC). The BBC comprises two arrays of 64 quartz Čerenkov counters covering pseudorapidity $3.0 < |\eta| < 3.9$. The MB trigger requires at least two hits in each of the BBC arrays and a reconstructed collision z -vertex of $|z| < 30$ cm, where $z = 0$ is the center of the detector. The BBC total charge is used as a measure of the collision centrality (the impact parameter of the Au+Au collision is monotonically related to the average total charged particle multiplicity). Following the procedure used for Au+Au at $\sqrt{s_{NN}} = 200$ GeV, for each centrality selection the average number of nucleon participants ($\langle N_{part} \rangle$) and the average number of binary collisions ($\langle N_{coll} \rangle$) are estimated using a Glauber model of the collision [25] and a negative binomial parametrization of the charged particles per pair of

*Deceased

†PHENIX Spokesperson: jacak@skipper.physics.sunysb.edu

participating nucleons. The total fraction of the Au+Au inelastic cross section measured by the MB trigger is determined to be $85.7 \pm 2.0\%$ and $85.9 \pm 2.0\%$ at 39 and 62.4 GeV, respectively. The minimum bias sample is divided into exclusive centrality bins that are categorized via the Glauber model comparison to the BBC charge distribution as given in Table I. Note that the centrality selections used here are wider than in previous analyses for Au+Au collisions at $\sqrt{s_{NN}} = 200$ GeV due to the smaller statistical sample of J/ψ s.

TABLE I: Mean N_{part} and N_{coll} values and systematic uncertainties in each centrality bin for Au+Au at 39 and 62.4 GeV.

$\sqrt{s}(\text{GeV})$	Cent(%)	$\langle N_{\text{part}} \rangle$	$\langle N_{\text{coll}} \rangle$
39	0-40	204.4 ± 4.4	444.8 ± 50.3
	40-86	34.1 ± 1.6	43.5 ± 3.7
62.4	0-20	274.8 ± 3.8	689.9 ± 78.9
	20-40	138.7 ± 4.7	270.5 ± 27.5
	40-60	59.7 ± 3.9	85.7 ± 9.1
	60-86	14.7 ± 1.2	14.3 ± 1.7

For each centrality selection and beam energy, we extract the number of J/ψ counts following a method identical to that used in Ref. [4]. All unlike-sign muon candidates are paired to calculate the invariant mass distribution. Underneath the J/ψ signal are continuum background counts both from uncorrelated tracks and from correlated physical backgrounds such as open charm decay (e.g. $D\bar{D}$ where both decay semi-leptonically to muons), open bottom decay, and the Drell-Yan process. First the uncorrelated background is calculated via an event mixing method with pairs from different Au+Au events with the same centrality and z -vertex. This background is then normalized using a comparison of real-event and mixed-event like-sign pairs. After subtraction of the uncorrelated background, we fit to the remaining correlated dimuon spectrum with an acceptance-modulated J/ψ line shape (determined from a full GEANT [26] simulation of the PHENIX detector) and an exponential folded with the acceptance to model the remaining correlated physics background. Utilizing different assumptions about the line shape, different uncorrelated background normalizations, and different invariant mass ranges for the fit (as detailed in Ref. [4]), we determine the systematic uncertainty on the extracted J/ψ signal counts. The total J/ψ sample corresponding to all centralities is approximately 170 counts at $\sqrt{s_{NN}} = 39$ GeV and approximately 1060 counts at $\sqrt{s_{NN}} = 62.4$ GeV. The invariant mass distribution of unlike-sign pairs, mixed-event pairs, and the subtracted distributions are shown in Figure 1. The signal extraction procedure is quite robust and the systematic uncertainty is of order 2-10%.

The J/ψ invariant yield is expressed as:

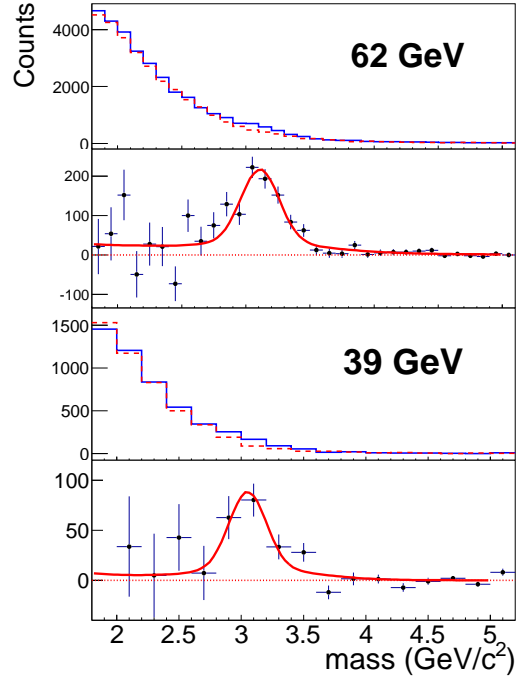


FIG. 1: (color online) The unlike sign invariant mass distribution (blue) for all Au+Au centralities and both muon arms is shown along with the uncorrelated background calculation from mixed event pairs (red) for 62 GeV (top two panels) and 39 GeV (bottom two panels). The lower panel in each pair shows the subtracted distribution and a fit to the data.

$$B_{\mu\mu} \frac{d^3N}{dp_T^2 dy} = \frac{1}{2\pi p_T \Delta p_T \Delta y} \frac{N_{J/\psi}}{A\epsilon N_{EVT}} \quad (1)$$

where $B_{\mu\mu}$ is the branching fraction of J/ψ to muons, $N_{J/\psi}$ is the number of measured J/ψ s, N_{EVT} is the number of events in the relevant Au+Au centrality selection, $A\epsilon$ is the detector geometric acceptance times efficiency, and Δp_T and Δy are the bin width in p_T and y , respectively. For the p_T -integrated bins, we similarly calculate $B_{\mu\mu} dN/dy = N_{J/\psi} / (A\epsilon N_{EVT} \Delta y)$. We evaluate the acceptance and reconstruction efficiency by running PYTHIA-generated [27] J/ψ s through the GEANT simulation of the PHENIX detector and then embedding these simulated hits into real Au+Au data events. These simulated events are then reconstructed using identical code to that used in the real data analysis, and the overall acceptance and efficiency ($A\epsilon$) is determined for each Au+Au centrality selection. In measurements at higher energy [4], where the multiplicity is larger, there are large drops in the efficiency for more central collisions; but for these lower energies, with their lower multiplicity, there is no significant loss of efficiency for central collisions. There is an additional check on the efficiency of each MuTr and MuID plane that is determined via a data-driven method. The invariant yields are calculated separately for each of the two muon spectrometers and then

a weighted average taken. These results agree within uncertainties in all cases.

Two categories of systematic uncertainties on the invariant yields are shown in Table II: type A are point-to-point uncorrelated, and type B are correlated (or anti-correlated) point-to-point. The uncertainties listed in order are from uncertainties on the J/ψ extracted yield as described above, the detector acceptance, the acceptance and efficiency over the rapidity range $1.2 < |y| < 2.2$ from the assumed PYTHIA input distribution, the absolute check on the MuTr and MuID hit efficiencies, and the matching of dead areas in the real data and GEANT Monte Carlo (MC) simulation.

TABLE II: Systematic uncertainties

Description	Contribution	Type
Yield extraction	2-10%	A
Detector acceptance	5%	B
Input y, p_T distribution	4%	B
MuTr efficiency	2%	B
MuID efficiency	4%	B
DATA and MC mismatch	4%	B

II. RESULTS

Figure 2 shows the final calculated J/ψ invariant yield integrated over all p_T in $\sqrt{s_{NN}} = 39$ and 62.4 GeV Au+Au collisions as a function of centrality, categorized by the average number of participants $\langle N_{part} \rangle$. The yields have been rescaled by $1/\langle N_{coll} \rangle$. For comparison, the previously published J/ψ invariant yields in the same rapidity range $1.2 < |y| < 2.2$ from $\sqrt{s_{NN}} = 200$ GeV Au+Au collisions are also shown [4]. The vertical error bars are the quadrature sum of the statistical and type A systematic uncertainties, and the boxes represent the type B uncertainties. As expected, the J/ψ yield is larger in Au+Au collisions at larger center-of-mass energy. In addition, the yield per binary collision is decreasing with $\langle N_{part} \rangle$ at all three energies, indicating increasing nuclear suppression for more central collisions. Figure 3 shows the invariant yield as a function of p_T , plotted at the center of each p_T bin, for $\sqrt{s_{NN}} = 39$ and 62.4 GeV Au+Au collisions.

The nuclear modification of J/ψ yields can be categorized in different ways. Because the PHENIX experiment has not yet measured the $p+p$ reference baselines at $\sqrt{s_{NN}} = 39$ or 62.4 GeV, we first discuss the J/ψ R_{CP} , the nuclear modification of central relative to peripheral classes of events as defined below:

$$R_{CP} = \frac{\frac{dN_{AuAu}/dy}{\langle N_{coll} \rangle}(central)}{\frac{dN_{AuAu}/dy}{\langle N_{coll} \rangle}(peripheral)} \quad (2)$$

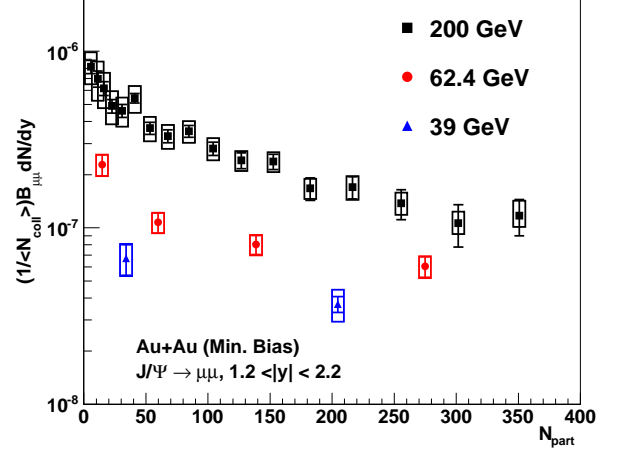


FIG. 2: (color online) J/ψ invariant yields (scaled by $1/\langle N_{coll} \rangle$) are shown for Au+Au collisions at 39, 62.4, and 200 GeV as a function of the number of participating nucleons. The solid error bars represent the uncorrelated point-to-point uncertainties (quadrature sum of statistical and type A); and the boxes represent the correlated (type B) systematic uncertainties.

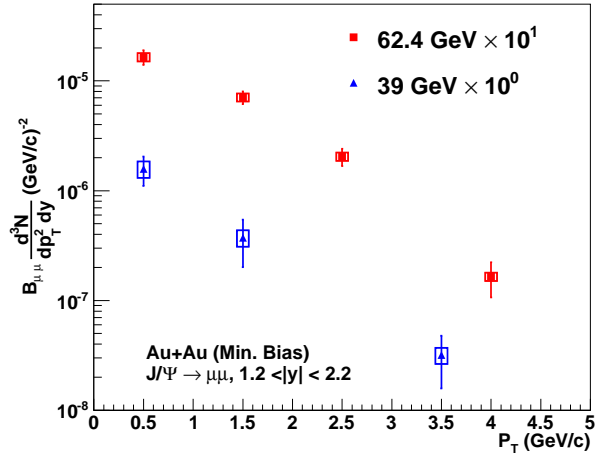


FIG. 3: (color online) J/ψ invariant yields in minimum bias Au+Au collisions at 39 and 62.4 GeV as a function of transverse momentum. The solid error bars are the quadrature sum of the statistical and type A systematic uncertainties, and the boxes represent the correlated (type B) systematic uncertainties.

The R_{CP} values are shown in Figure 4 and in Table III for Au+Au at 62.4 GeV. Note that the peripheral bin selection for Au+Au at 62.4 GeV is 60-86% centrality with a corresponding $\langle N_{coll} \rangle = 14.3 \pm 1.7$. Many uncertainties in the invariant yields cancel for R_{CP} and the dominant uncertainties are from the normalization with respect to the peripheral bin including the uncertainties in the $\langle N_{coll} \rangle$ values for each bin. There is an additional

type C global systematic from the uncertainty in the peripheral $\langle N_{\text{coll}} \rangle$ value listed in the figure legend and in Table III; the other systematic uncertainties are included in the boxes on each data point. For comparison, we show the published Au+Au results at 200 GeV [4] where the peripheral selection is 60-93%, with a quite comparable $\langle N_{\text{coll}} \rangle = 14.5 \pm 2.7$. Within uncertainties, the centrality-dependent nuclear modification from peripheral to central collisions at the two energies are the same.

TABLE III: PHENIX 39 and 62.4 GeV J/ψ R_{CP} vs Centrality with statistical uncertainties and Type A, B, and C systematics.

$\sqrt{s}(\text{GeV})$	Cent(%)	R_{CP}	Stat	Type A	Type B	Type C
39	0-40	0.554	0.112	0.028	0.138	0.047
62.4	0-20	0.266	0.050	0.005	0.036	0.031
	20-40	0.353	0.064	0.008	0.045	0.041
	40-60	0.471	0.089	0.013	0.060	0.055

For the Au+Au results at 39 GeV, the statistics do not allow any centrality dependence of R_{CP} and only a single value is calculated for the ratio between 0-40% to 40-86% centralities, as shown in Figure 5 and in Table III. The published Au+Au results at 200 GeV are rebinned to have a peripheral centrality selection of 40–93% to approximately match the number of binary collisions for the peripheral denominator. Within uncertainties the results agree; however, the limited statistics in the Au+Au at 39 GeV preclude any strong conclusions.

The centrality dependence as quantified via R_{CP} is not a replacement for the nuclear modification factor R_{AA} (relative to the $p+p$ baseline) since J/ψ yields may change already in peripheral Au+Au collisions, in particular from cold nuclear matter effects. In addition, R_{CP} has significant uncertainties from the more limited statistics and the larger systematic uncertainty on $\langle N_{\text{coll}} \rangle$ for the peripheral bin. The PHENIX experiment has no data for $p+p$ collisions at 39 GeV, and only a limited data set was recorded during 2006 for $p+p$ collisions at 62.4 GeV. However, $p+p$ measurements do exist from fixed target $p+A$ experiments near 39 GeV and from ISR collider experiments at 62 GeV. In the Appendix, we discuss in detail these results and compare them with theoretical calculations within the Color Evaporation Model (CEM) from R. Vogt [28, 29] to determine a $p+p$ reference.

We quantify the nuclear modification factor R_{AA} with respect to the $p+p$ reference as follows:

$$R_{AA} = \frac{1}{\langle T_{AA} \rangle} \frac{dN^{AA}/dy}{d\sigma^{pp}/dy} \quad (3)$$

where dN^{AA}/dy is the invariant yield in Au+Au collisions, $d\sigma^{pp}/dy$ is the $p+p$ cross section, and $\langle T_{AA} \rangle$ is the nuclear overlap function (where $\langle T_{AA} \rangle = \langle N_{\text{coll}} \rangle / \sigma_{NN}^{\text{inelastic}}$). Unlike 200 GeV, the 39 and 62 GeV

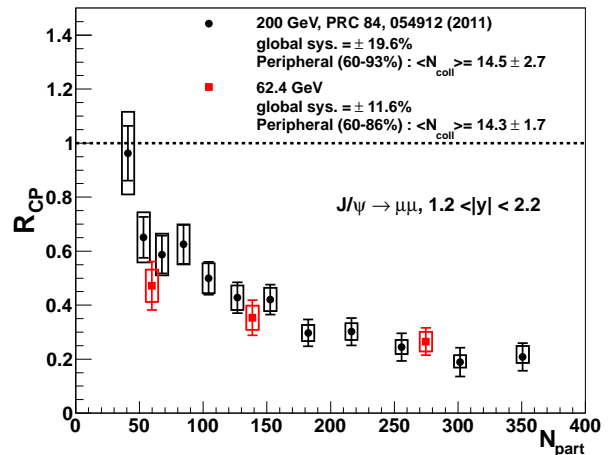


FIG. 4: (color online) J/ψ R_{CP} for 0-20%, 20-40%, and 40-60% (central) relative to 60-86% (peripheral) Au+Au collisions at 62.4 GeV. For comparison, R_{CP} results from Au+Au collisions at 200 GeV are shown with a peripheral bin of 60-93%, where the $\langle N_{\text{coll}} \rangle$ value is a close match. The solid error bars are the quadrature sum of the statistical and type A systematic uncertainties, and the boxes represent the correlated (type B) systematic uncertainties.

$p+p$ references are determined from other measurements rather than being from our own, and systematic uncertainties will not cancel in the ratio. Our estimates for the J/ψ $p+p$ cross sections in the range $1.2 < |y| < 2.2$ for 39 and 62.4 GeV are shown in Table IV, and are detailed in the Appendix. The J/ψ R_{AA} for Au+Au collisions at 39 and 62.4 GeV is tabulated in Table V and shown in Figure 6 as a function of the number of participating nucleons $\langle N_{\text{part}} \rangle$, along with the previously published 200 GeV results [4]. The type C global scale uncertainties, from the $p+p$ references, are listed separately in the legend. At both 39 and 62.4 GeV, there is slightly less J/ψ suppression than observed in Au+Au at 200 GeV. However, particularly for 62.4 GeV, since we have no reliable $p+p$ reference from our own measurements, the R_{AA} result could shift down by the quoted 29% systematic uncertainty, bringing the data into agreement with the 200 GeV result.

TABLE IV: Estimates used for the 39 and 62.4 GeV J/ψ $p+p$ cross sections along with their uncertainties. See the Appendix for details.

$\sqrt{s}(\text{GeV})$	$d\sigma^{pp}/dy$
39	$2.91 \pm 19\%$ nb
62.4	$7.66 \pm 29.4\%$ nb

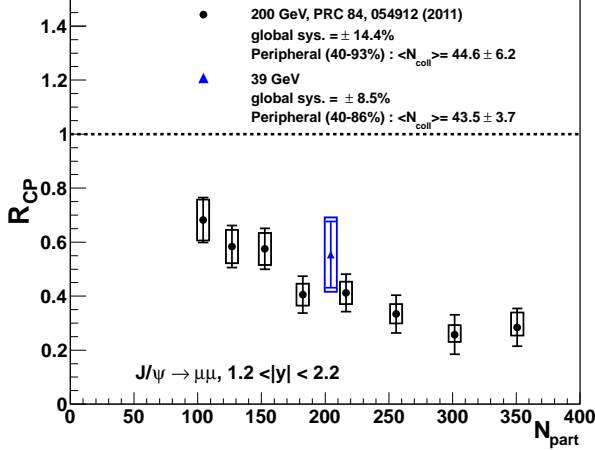


FIG. 5: (color online) J/ψ R_{CP} for 0-40% (central) relative to 40-87% (peripheral) Au+Au collisions at 39 GeV. For comparison, R_{CP} results from Au+Au collisions at 200 GeV are shown with a peripheral bin of 40-93%, where the $\langle N_{coll} \rangle$ value is a close match. The solid error bars are the quadrature sum of the statistical and type A systematic uncertainties, and the boxes represent the correlated (type B) systematic uncertainties.

TABLE V: PHENIX 39 and 62.4 GeV J/ψ R_{AA} vs Centrality with statistical uncertainties and Type A, B and C systematics.

$\sqrt{s}(GeV)$	Cent(%)	R_{AA}	Stat	Type A	Type B	Type C
39	0-40	0.439	0.043	0.020	0.077	0.083
	40-86	0.793	0.157	0.011	0.139	0.151
62.4	0-20	0.292	0.039	0.004	0.042	0.085
	20-40	0.388	0.047	0.008	0.056	0.115
	40-60	0.519	0.067	0.014	0.073	0.153
	60-86	1.100	0.150	0.010	0.155	0.323

III. DISCUSSION

The collision energy dependence of the various competing effects influencing the final J/ψ yields are all quite different. Thus, the similarity of the J/ψ nuclear modifications R_{CP} and R_{AA} from 39 to 200 GeV is a challenge for models incorporating the many effects. There was a prediction that the maximum J/ψ suppression would occur near $\sqrt{s_{NN}} = 50$ GeV, as shown in Figure 7 [30]. As the collision energy increases the QGP temperature increases, and thus the J/ψ color screening (labeled as direct J/ψ suppression) becomes more significant. However, in this calculation, the regeneration contribution increases with collision energy due to the increase in the total number of charm pairs produced and nearly compensates. This result is for J/ψ at midrapidity and relative to the total charm pair production (thus removing in

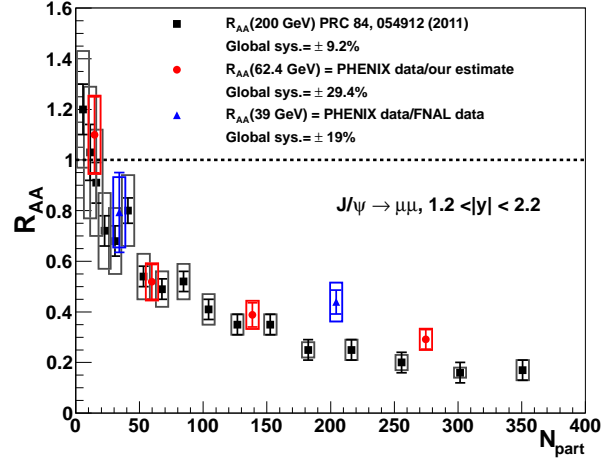


FIG. 6: (color online) J/ψ R_{AA} at $\sqrt{s_{NN}} = 39, 62.4$, and 200 GeV. The solid error bars are the quadrature sum of the statistical and type A systematic uncertainties, and the boxes represent the correlated (type B) systematic uncertainties. The global systematic uncertainties are quoted in the legend for each energy's results.

this ratio possible changes in the charm pair production caused by initial state effects).

Recently, the same authors have completed new calculations including cold nuclear matter effects, regeneration, and QGP suppression specifically for J/ψ at forward rapidity [31, 32]. Figure 8 shows these results (in the so-called “strong binding scenario”). The contributions of direct J/ψ and regeneration are shown separately (and scaled down by $\times 0.5$ for visual clarity). The inclusion of cold nuclear matter effects and the forward-rapidity kinematics slightly reverse the trend seen in Figure 7 and now the total J/ψ R_{AA} follows the ordering $R_{AA}(200 \text{ GeV}) < R_{AA}(62 \text{ GeV}) < R_{AA}(39 \text{ GeV})$ (though by a very modest amount). Also shown in Figure 8 are the PHENIX experimental measurements that, within the global systematic uncertainties, are consistent with the theoretical calculations.

These results highlight the need for $p+p$ reference data at both 39 and 62.4 GeV from the same experiment. In addition, the cold nuclear matter effects are likely to be different at the different energies (an important input for the calculations in Ref. [31]). The x distribution of gluons for producing J/ψ at $1.2 < |y| < 2.2$ changes as the colliding energy decreases. In a simple PYTHIA study, one finds that the average gluon x_1 and x_2 for producing J/ψ between $1.2 < |y| < 2.2$ is 0.14 and 0.01 for $\sqrt{s_{NN}} = 200$ GeV, 0.32 and 0.03 for $\sqrt{s_{NN}} = 62.4$ GeV, and 0.43 and 0.05 for $\sqrt{s_{NN}} = 39$ GeV. The large uncertainties in the gluon nPDF for the anti-shadowing and EMC regions [9] leads to an additional $\pm 30\%$ uncertainty in the J/ψ initial production for the central Au+Au case. Future measurements in $p(d)+A$ collisions at these energies are clearly required in order to reduce this large

IV. SUMMARY

The PHENIX experiment has measured the invariant yield of J/ψ at forward rapidity in Au+Au collisions at 39 and 62.4 GeV. The nuclear modification, when formulated as R_{CP} (the ratio between central and peripheral event classes), indicates a similar suppression pattern at the two lower energies to that previously published for Au+Au collisions at 200 GeV. Using a $p+p$ reference from other experiments and from a Color Evaporation Model calculation, results in an R_{AA} with slightly less suppression at these lower energies. These results are consistent with theoretical calculations dominated by the balancing effects of more QGP suppression as well as more J/ψ regeneration for high-energy collisions. However, any firm conclusion regarding the overall level of suppression from the QGP requires additional $p+p$ and $p(d)+A$ data at these energies.

V. ACKNOWLEDGMENTS

We thank the staff of the Collider-Accelerator and Physics Departments at Brookhaven National Laboratory and the staff of the other PHENIX participating institutions for their vital contributions. We acknowledge support from the Office of Nuclear Physics in the Office of Science of the Department of Energy, the National Science Foundation, Abilene Christian University Research Council, Research Foundation of SUNY, and Dean of the College of Arts and Sciences, Vanderbilt University (U.S.A), Ministry of Education, Culture, Sports, Science, and Technology and the Japan Society for the Promotion of Science (Japan), Conselho Nacional de Desenvolvimento Científico e Tecnológico and Fundação de Amparo à Pesquisa do Estado de São Paulo (Brazil), Natural Science Foundation of China (P. R. China), Ministry of Education, Youth and Sports (Czech Republic), Centre National de la Recherche Scientifique, Commissariat à l'Énergie Atomique, and Institut National de Physique Nucléaire et de Physique des Particules (France), Bundesministerium für Bildung und Forschung, Deutscher Akademischer Austausch Dienst, and Alexander von Humboldt Stiftung (Germany), Hungarian National Science Fund, OTKA (Hungary), Department of Atomic Energy and Department of Science and Technology (India), Israel Science Foundation (Israel), National Research Foundation and WCU program of the Ministry Education Science and Technology (Korea), Ministry of Education and Science, Russian Academy of Sciences, Federal Agency of Atomic Energy (Russia), VR and Wallenberg Foundation (Sweden), the U.S. Civilian Research and Development Foundation for the Independent States of the Former Soviet Union, the Hungarian American Enterprise Scholarship Fund, and the US-Israel Binational Science Foundation.

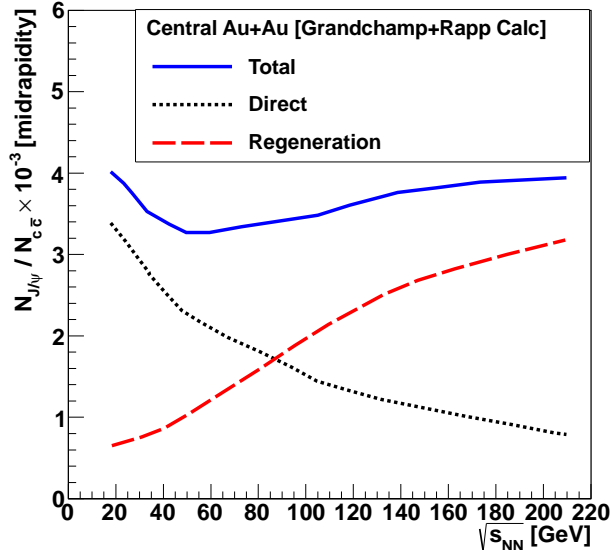


FIG. 7: (color online) The number of J/ψ per produced charm pair ($\times 10^{-3}$) in Au+Au central collisions ($N_{\text{part}} = 360$) at midrapidity. Shown are the direct J/ψ and regeneration contributions. Calculation details and figure from [30].

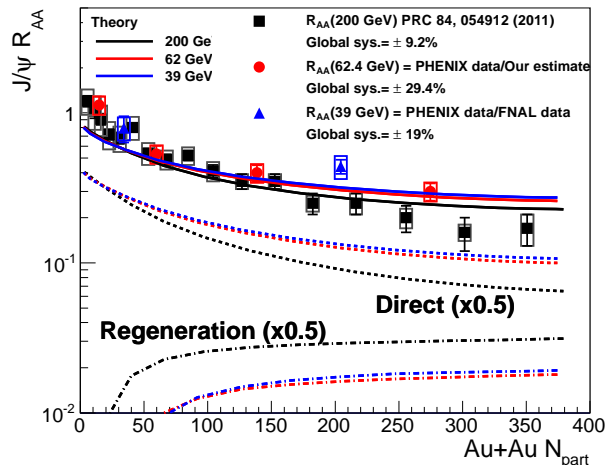


FIG. 8: (color online) The J/ψ nuclear modification factor R_{AA} as a function of the number of participating nucleons N_{part} for $\sqrt{s_{NN}} = 39, 62.4, 200$ GeV Au+Au collisions. Calculation results are shown from [31] for the total J/ψ R_{AA} and the separate contribution of direct J/ψ suppression and regeneration (scaled down by $\times 0.5$ for visual clarity). The PHENIX experimental data points are shown for comparison.

uncertainty contribution.

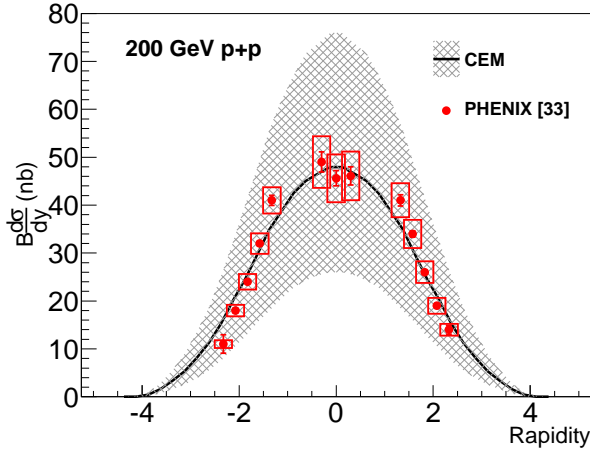


FIG. 9: (color online) J/ψ cross section as a function of rapidity in $p+p$ collisions at 200 GeV. The CEM calculation is shown as a black solid line with a gray band for its uncertainty. In comparison, PHENIX measurements are shown as red points [33].

Appendix: Proton-Proton Reference

In order to construct the $p+p$ references at 39 and 62.4 GeV, we utilize lower-energy data from Fermilab and the ISR, and also the Color Evaporation Model (CEM) calculations from R. Vogt [28, 29]. These calculations have been extensively compared with J/ψ cross sections as a function of center-of-mass energy. First, shown in Figure 9 is a comparison of the published PHENIX measurements for the J/ψ cross section in $p+p$ collisions at 200 GeV [33] and the CEM calculation. For the CEM calculation, the solid line is the central value and the gray band represents the systematic uncertainty of the results. Using the same CEM framework, calculation results for $p+p$ at 39 and 62.4 GeV are shown in Figs. 10 and 11, respectively. It is notable that the predicted cross section at midrapidity drops by approximately a factor of 2.5 in going from 200 to 62.4 GeV, and then another factor of 1.9 in going from 62.4 to 39 GeV. The rapidity distribution also narrows as expected.

1. $p+p$ at 39 GeV

Fermilab fixed target experiment E789 [34, 35] has measured the invariant cross sections of J/ψ in $p+\text{Be}$, $p+\text{Cu}$, and $p+\text{Au}$ collisions over a broad rapidity range at $\sqrt{s_{NN}} = 38.8$ GeV. The rapidity coverage for $p+\text{Au}$ was $-0.1 < y < +0.7$; and for $p+\text{Be}$ and $p+\text{Cu}$ was $1.4 < y < 2.4$. In addition, the nuclear dependence of the cross sections was measured by E866/NuSea [15] and found to follow the functional form, $\sigma_{p+A} = A^\alpha \sigma_{p+p}$, where,

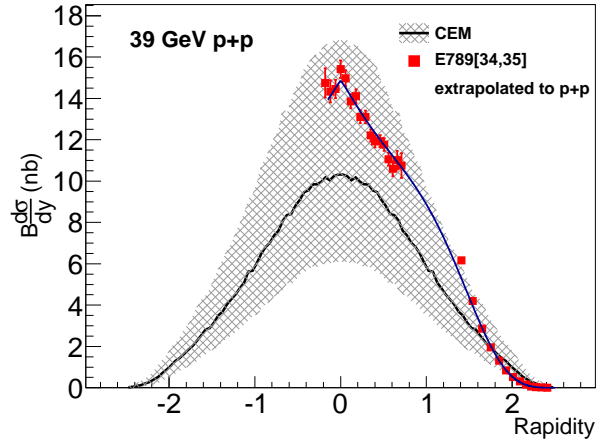


FIG. 10: (color online) J/ψ cross section as a function of rapidity in $p+p$ collisions at 39 GeV. The CEM calculation is shown as a black solid line with a gray band for its uncertainty. Data points and fit function are the result of the $p+A$ data extrapolation to $p+p$ as described in the text.

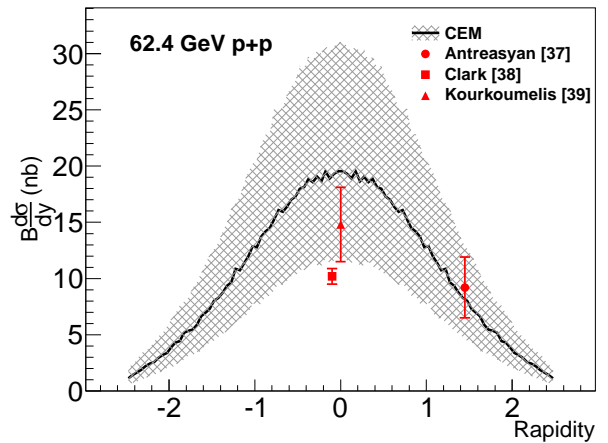


FIG. 11: (color online) J/ψ cross section as a function of rapidity in $p+p$ collisions at 62.4 GeV. The CEM calculation is shown as a black solid line with a gray band for its uncertainty. Data points from ISR measurements are shown as detailed in the text.

$$\alpha(x_F) = 0.960(1 - 0.0519x_F - 0.338x_F^2) \quad (\text{A.1})$$

(as seen in Figures 2 and 3 of Ref. [15]).

Using this parametrization for the nuclear dependence, one can extrapolate versus A from the $p+A$ J/ψ cross sections to those for $p+p$ ($A = 1$) and obtain the $p+p$ cross sections as a function of x_F . After converting these to be versus rapidity, they are shown in Figure 10. For the rapidity range $1.2 < y < 2.2$ one obtains $2.91 \pm 19\%(\text{syst})$ nb by integrating the fit function. In comparison, the result from the CEM calculation

is $2.45^{+1.78}_{-1.0}$ nb, which agrees well within uncertainties. Thus, we use this extraction from the experimental data for the 39 GeV $p+p$ reference, as shown in Table IV. Systematic uncertainties on this reference include 12% from the E789 $p+A$ data and 15% to account for the quality of the fit and for its extrapolation in rapidity into the unmeasured $1.2 < y < 1.4$ region.

2. $p+p$ at 62.4 GeV

Experiments at the CERN Intersecting Storage Ring (ISR) measured the J/ψ cross section in $p+p$ collisions at 62 GeV [36–38]. These results are shown in Table VI and in comparison to the CEM calculation in Figure 11. Since our measurements lie in the rapidity range $1.2 < |y| < 2.2$, the most important $p+p$ measurement from the ISR for our purposes is that of Antreasyan [36], which covers a rapidity range of $0.89 < y < 1.82$ and agrees quite well with the CEM calculation. Therefore we estimate the $p+p$ reference by integrating over our ra-

pidity coverage using the CEM calculation fitted to the Antreasyan measurement. For the uncertainties of this reference we take similar CEM guided integrals, but constrained to the upper and to the lower limits of the that ISR measurement. This results in a 62 GeV $p+p$ reference of $7.66 \pm 29.4\%$ nb. We note that the midrapidity ISR points are somewhat low but nearly consistent with the CEM calculation, but since our data lies at large rapidity we rely on the Antreasyan ISR point.

TABLE VI: ISR measurements of J/ψ in $p+p$ collisions at 62 GeV

Reference	Rapidity Range	$B_{ee} \frac{d\sigma}{dy} (\text{nb})$
Antreasyan <i>et al.</i> [36]	$0.89 < y < 1.82$	9.21 ± 2.70
Clark <i>et al.</i> [37]	$ y < 0.5$	10.2 ± 0.7
Kourkouvelis <i>et al.</i> [38]	$ y < 0.65$	14.8 ± 3.3

-
- [1] T. Matsui and H. Satz, Phys. Lett. B **178**, 416 (1986).
 - [2] M. Abreu *et al.* (NA50 Collaboration), Phys. Lett. B **477**, 28 (2000).
 - [3] A. Adare *et al.* (PHENIX Collaboration), Phys. Rev. Lett. **98**, 232301 (2007).
 - [4] A. Adare *et al.* (PHENIX Collaboration), Phys. Rev. C **84**, 054912 (2011).
 - [5] B. Abelev *et al.* (ALICE Collaboration), arXiv:1202.1383 (2012).
 - [6] G. Aad *et al.* (ATLAS Collaboration), Phys. Lett. B **697**, 294 (2011).
 - [7] S. Chatrchyan *et al.* (CMS Collaboration), JHEP **1205**, 063 (2012), 1201.5069.
 - [8] Z. Tang (STAR Collaboration), J. Phys. G **38**, 124107 (2011), 1107.0532.
 - [9] K. J. Eskola, H. Paukkunen, and C. A. Salgado, JHEP **04**, 065 (2009).
 - [10] M. Abreu *et al.* (NA38 Collaboration), Phys. Lett. B **444**, 516 (1998).
 - [11] B. Alessandro *et al.* (NA50 Collaboration), Phys. Lett. B **553**, 167 (2003).
 - [12] B. Alessandro *et al.* (NA50 Collaboration), Eur. Phys. J. C **33**, 31 (2004).
 - [13] B. Alessandro *et al.* (NA50 Collaboration), Eur. Phys. J. C **48**, 329 (2006).
 - [14] R. Arnaldi *et al.* (NA60 Collaboration), Phys. Lett. B **706**, 263 (2012).
 - [15] M. J. Leitch *et al.* (FNAL E866/NuSea Collaboration), Phys. Rev. Lett. **84**, 3256 (2000).
 - [16] I. Abt *et al.* (HERA-B Collaboration), Eur. Phys. J. C **60**, 525 (2009).
 - [17] A. Adare *et al.* (PHENIX Collaboration), Phys. Rev. Lett. **107**, 142301 (2011), 1010.1246.
 - [18] A. Adare *et al.* (PHENIX Collaboration).
 - [19] J. Nagle, A. Frawley, L. L. Levy, and M. Wysocki, Phys. Rev. C **84**, 044911 (2011).
 - [20] R. L. Thews and M. L. Mangano, Phys. Rev. C **73**, 014904 (2006).
 - [21] K. Zhou, N. Xu, and P. Zhuang, Nucl. Phys. A **834**, 249C (2010).
 - [22] N. Brambilla, S. Eidelman, B. Heltsley, R. Vogt, G. Bodwin, *et al.*, Eur. Phys. J. C **71**, 1534 (2011).
 - [23] K. Adcox *et al.* (PHENIX Collaboration), Nucl. Inst. and Meth. A **499**, 469 (2003).
 - [24] S. Aronson *et al.* (PHENIX Collaboration), Nucl. Inst. and Meth. A **499**, 480 (2003).
 - [25] M. L. Miller, K. Reygers, S. J. Sanders, and P. Steinberg, Annu. Rev. Nucl. Part. Sci. **57**, 205 (2007).
 - [26] R. Brun *et al.*, CERN Program Library Long Write-up W5013 (1994), URL <http://wwwasd.web.cern.ch/wwwasd/geant/>.
 - [27] T. Sjöstrand, P. Edén, C. Friberg, L. Lönnblad, G. Miu, S. Mrenna, and E. Norrbin, Comput. Phys. Commun. **135**, 238 (2001).
 - [28] A. Frawley, T. Ullrich, and R. Vogt, Phys. Rep. **462**, 125 (2008).
 - [29] R. Vogt, private communication (2012).
 - [30] L. Grandchamp and R. Rapp, Nucl. Phys. A **709**, 415 (2002).
 - [31] X. Zhao and R. Rapp, Phys. Rev. C **82**, 064905 (2010).
 - [32] X. Zhao and R. Rapp, private communication (2012).
 - [33] A. Adare *et al.* (PHENIX Collaboration), Phys. Rev. D **85**, 092004 (2012).
 - [34] M. H. Schub *et al.*, Phys. Rev. D **52**, 1307 (1995).
 - [35] M. S. Kowitt *et al.*, Phys. Rev. Lett. **72**, 1318 (1994).
 - [36] D. Antreasyan *et al.*, Phys. Rev. Lett. **48**, 302 (1982).
 - [37] A. G. Clark *et al.*, Nucl. Phys. B **142**, 29 (1978).
 - [38] C. Kourkouvelis *et al.*, Physics Letters B **91**, 481 (1980).